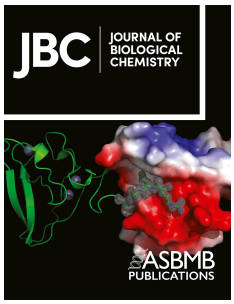

Discovery of a novel lactate dehydrogenase tetramerization domain using epitope mapping and peptides

Léopold Thabault, Maxime Liberelle, Katarina Koruza, Esra Yildiz, Nicolas Joudiou, Joris Messens, Lucie Brisson, Johan Wouters, Pierre Sonveaux, Raphaël Frédérick

PII: S0021-9258(21)00195-2

DOI: https://doi.org/10.1016/j.jbc.2021.100422

Reference: JBC 100422

To appear in: *Journal of Biological Chemistry*

Received Date: 5 January 2021

Revised Date: 8 February 2021

Accepted Date: 12 February 2021

Please cite this article as: Thabault L, Liberelle M, Koruza K, Yildiz E, Joudiou N, Messens J, Brisson L, Wouters J, Sonveaux P, Frédérick R, Discovery of a novel lactate dehydrogenase tetramerization domain using epitope mapping and peptides, *Journal of Biological Chemistry* (2021), doi: https://doi.org/10.1016/j.jbc.2021.100422.

Discovery of a novel lactate dehydrogenase tetramerization domain using epitope mapping and peptides

Léopold Thabault,[1,2] Maxime Liberelle,[1] Katarina Koruza,[3,4,5] Esra Yildiz,[1] Nicolas Joudiou,[6] Joris Messens,[3,4,5] Lucie Brisson,[7] Johan Wouters,[8] Pierre Sonveaux,[*,$,2] Raphaël Frédérick[*,$,1]

[1] Louvain Drug Research Institute (LDRI), Université catholique de Louvain (UCLouvain), B-1200 Brussels, Belgium.
[2] Pole of Pharmacology and Therapeutics, Institut de Recherche Expérimentale et Clinique (IREC), Université catholique de Louvain (UCLouvain),B-1200 Brussels, Belgium.
[3] VIB-VUB Center for Structural Biology, B-1050 Brussels, Belgium.
[4] Brussels Center for Redox Biology, B-1050 Brussels, Belgium.
[5] Structural Biology Brussels, Vrije Universiteit Brussel, B-1050 Brussels, Belgium.
[6] Nuclear and Electron Spin Technologies, Louvain Drug Research Institute (LDRI), Université catholique de Louvain (UCLouvain), B-1200 Brussels, Belgium.
[7] Inserm UMR1069, Nutrition, Growth and Cancer, University of Tours, Tours, France.
[8] NARILIS, Department of Chemistry, UNamur, University of Namur, B-5000 Namur, Belgium.
[$] R.F. and P.S. are co-senior authors.

*Corresponding authors: Pierre Sonveaux − Pole of Pharmacology and Therapeutics, Institut de Recherche Expérimentale et Clinique (IREC), Université Catholique de Louvain, B-1200 Brussels, Belgium; Email: pierre.sonveaux@uclouvain.be

Raphaël Frédérick − Louvain Drug Research Institute (LDRI), Université Catholique de Louvain, B-1200 Brussels, Belgium; Email: raphael.frederick@uclouvain.be

Running title: Discovery of a lactate dehydrogenase tetramerization domain

Key-words: Cancer; Peptides; Biophysics; Oligomerization; Protein-protein interaction; Nuclear magnetic resonance (NMR); Mass photometry; MicroScale Thermophoresis; NanoDSF; Lactate dehydrogenases; Disruptors.

Abstract

Despite being initially regarded as a metabolic waste product, lactate is now considered to serve as a primary fuel for the tricarboxylic acid (TCA) cycle in cancer cells. At the core of lactate metabolism, lactate dehydrogenases (LDHs) catalyze the interconversion of lactate to pyruvate and as such represent promising targets in cancer therapy. However, direct inhibition of the LDH active site is challenging from physicochemical and selectivity standpoints. However, LDHs are obligate tetramers. Thus, targeting the LDH tetrameric interface has emerged as an appealing strategy. In this work, we examine a dimeric construct of truncated human LDH to search for new druggable sites. We report the identification and characterization of a new cluster of interactions in the LDH tetrameric interface. Using nanoscale differential scanning fluorimetry, chemical denaturation and mass photometry, we

identified several residues (E62, D65, L71 and F72) essential for LDH tetrameric stability. Moreover, we report a family of peptide ligands based on this cluster of interactions. We next demonstrated these ligands to destabilize tetrameric LDHs through binding to this new tetrameric interface using nanoscale differential scanning fluorimetry, nuclear magnetic resonance water-ligand observed via gradient spectroscopy and microscale thermophoresis. Altogether, this work provides new insights on the LDH tetrameric interface as well as valuable pharmacological tools for the development of LDH tetramer disruptors.

Introduction

Dysregulation of glucose metabolism is a common feature of most cancer cells.[1] The elevated glycolytic flux in cancer cells has two origins: adaptation to hypoxia (anaerobic glycolysis) and adaptation to high proliferation rates (aerobic glycolysis, also known as the "Warburg effect")[2]. This higher glycolytic flux provides cancer cells with the energy and biomass essential for the sustainment of their anabolic growth. At the end of the glycolytic pathway stands the reduction of pyruvate to lactate catalyzed by the lactate dehydrogenase (LDH) family.

While lactate has long been considered as a mere by-product of glycolysis, it is now regarded as a potential purpose of accelerated glycolysis in cancer, in the light of the numerous benefits it provides to tumor growth.[3] Elevation of lactate production indeed promotes several phenomena such as angiogenesis,[4–6] invasiveness,[7,8] commensalism,[9] inflammation[10,11] as well as redox homeostasis.[12] Lactate metabolism further establishes a metabolic symbiosis between oxidative cancer cells that use lactate preferentially to glucose as a fuel, and glycolytic cancer cells that rapidly convert glucose to lactate.[13] Lactate oxidation to pyruvate by LDHs further promotes lysosomal acidification and autophagy.[14]

LDHs are key enzymes at the core of this adaptive metabolism as they catalyze the terminal reaction of lactate biosynthesis with the interconversion of pyruvate and NADH to lactate and NAD^+. LDHs function as obligate tetramers constituted by the homo or hetero association of two isoenzymes, LDH-H (encoded by the *LDHB* gene) and LDH-M (encoded by the *LDHA* gene).[15] These two isoenzymes show very high homology and identity.[16] The two LDH homotetramers, LDH-1 (LDH-H_4) and LDH-5 (LDH-M_4), are the most extensively studied forms of LDH and constitute appealing targets for cancer therapy.[17,18]

Intense efforts were initially devoted to selective LDH-5 inhibition due to its broad implication in cancer pathogenesis.[19,20] However, more recent reports about the implications of LDH-1 in cancer pathogenesis shed light on LDH-1 inhibition. First, LDH-1 was reported to interact with lysosomal vesicular ATPase, thus regulating autophagy, and is essential for metabolic reprogramming through p53 and Ras mutations.[14,21] Second, the *LDHB* gene was identified to be essential for triple-negative breast cancer.[22] Finally, it has been shown that one LDH isoenzyme can compensate for the genetic disruption of the other in order to sustain the Warburg phenotype.[23] Altogether, these studies support the idea that dual LDH inhibitors could bring an additional therapeutic value over selective isoenzyme inhibition.

The therapeutic interest for LDH inhibition prompted the development of potent, dual or selective, active-site LDH inhibitors.[24–30] However, despite intense efforts, pharmacological LDH inhibition struggled to translate to *in vivo* activity.[27,29,31,32] In fact, LDHs are usually recognized as poorly druggable targets, and different reasons can account for this. First, LDH active-site inhibitors face a challenge in achieving selectivity over other dehydrogenases, notably due to a common NAD-binding domain. For instance, gossypol derivatives, that are among the first LDH inhibitors reported,[20] demonstrated significant inhibition towards other dehydrogenases.[33] Second, the LDH catalytic-site presents non-optimal physicochemical properties with high solvent exposure and hydrophilicity, leading to challenging absorption, distribution, metabolization and excretion (ADME) properties for most LDH active site inhibitors.[27,29,34] Finally, an inherent difficulty in achieving therapeutic LDH inhibition stems from its high intracellular concentration; LDHs are indeed highly

concentrated in cancer cells, with protein concentrations reported in the µM range.[29] This high cellular concentration often hampers the observation of cell-based inhibition below that µM threshold, even for the more potent nanomolar inhibitors reaching micromolar concentrations in tumours.[29,32]

These different challenges to LDH inhibition called for developing new strategies to target this enzymatic family of high therapeutic potential. To this end, tool compounds able to target the LDH oligomeric interface instead of its active site have been recently developed.[16,35–37] Targeting a protein oligomeric state is still an underexplored strategy that can provide several benefits over active-site targeting, and could thus overcome the existing difficulties encountered with LDH orthosteric inhibitors. Targeting LDH self-assembly could indeed lead to the identification of new and potentially more druggable allosteric sites.[16] Noteworthy, as LDH subunits can form homo- and heterotetramers, the tetrameric interface is shared between the two different isoenzymes. Targeting LDH tetrameric interface can thus yield to molecules disrupting both LDH-1 and LDH-5, which is in line with the current pan-LDH inhibition strategy.[16] Moreover, disruptors of protein self-assembly can induce protein misfolding and degradation.[38,39] Therefore, targeting the LDH oligomeric state could reduce its intracellular concentration, leading to sub-stoichiometric inhibition, hence higher efficacy.

To this end, we previously developed and characterized a dimeric model of LDH-H by truncating its N-terminal tetramerization domain (LDH-Htr).[16] This model allows to study the LDH tetrameric interface, and previously led to the identification of a first allosteric site involving the N-terminal residues. The present study report on the existence of a second allosteric site, based on which we developed a new family of peptidic ligands functioning as LDH inhibitors.

Results and Discussion

In silico mapping of the LDH-1 tetrameric interface identifies a new cluster of interactions

LDH quaternary state is a "dimer of dimers" (**Figure 1a**).[40,41] According to X-ray structures, three different subunit orientations could account for LDH dimeric conformation. We have indeed previously found that LDH N-terminal domain truncation leads to dimers (LDH-Htr) (**Figure 1a**).[16] In agreement with previous studies,[35] only the association of dimers A-C and B-D in a tetramer can explain the role of this N-terminal domain in the stabilization of the tetrameric state (**Figure 1a**). Based on this hypothesis, we first mapped the interactions made by one subunit with a LDH dimer (A-C or B-D) using the Molecular Operating Environment (MOE) software.[42] Mapping these contact points highlighted two clusters: **A** (**A_1** and **A_2**) and **B** (**B_1** and **B_2**) (**Figure 1b**). Cluster **A_1** and **A_2** corresponded to the LDH N-terminal tetramerization domain (**Figure 1c**) and to its related tetramerization site, respectively, which were previously investigated.[16] Clusters **B_1** and **B_2** matched with a 22 amino acid α-helix and its interacting site, which to our knowledge were never reported before. Interestingly, the sequence corresponding to cluster **B_1** was highly conserved among vertebrates (**Figure S1**). Overall, Clusters **A_1,** and **B_1** corresponded to continuous epitopes interacting with discontinuous oligomerization sites **A_2** and **B_2**.

LDH-Htr behaves as a weak tetramer through cluster B.

Next, we aimed to confirm this interaction model and the anticipated symmetry axis of LDH dimers using our model of dimeric LDH (LDH-Htr).[16] According to the interaction map, LDH-Htr lacks cluster **A_1**

but still possesses clusters **A_2**, **B_1**, and **B_2**. We thus reasoned that LDH-Htr might still be able to self-interact at high concentrations *via* cluster **B**. Comparison between LDH-Htr and LDH-1 elution profiles by size-exclusion chromatography (SEC) indeed suggested that LDH-Htr could be in an equilibrium between tetramers and dimers.[16] Consistently, the evaluation of LDH-Htr self-interaction by Microscale thermophoresis (MST) revealed that the dimeric protein interacts with itself at high concentrations (**Figure 2a**, K_d = 1.25 µM [0.96 to 1.62 µM]). According to our model, this interaction can only be the result of LDH-Htr forming dimers of dimers through cluster **B**. Monitoring this interaction using MST hence provided valuable information on cluster **B**'s overall potency. We then evaluated whether LDH-Htr self-association could stabilize the protein complex, as the oligomerization of a protein often results in its stabilization.[43] LDH-Htr denaturation profile was evaluated using nanoscale differential scanning fluorimetry (nanoDSF) and revealed that the protein exhibited a concentration-dependent destabilization (**Figure 2b**) and conformational change (**Figure 2c**). We also evaluated LDH-Htr oligomeric state using mass photometry (MP). MP is a recent technique that allows for single-molecule detection and mass measurement in solution based on light scattering.[44] MP analysis of LDH-Htr revealed an equilibrium between dimers and tetramers in solution (**Figure 2d**). Altogether, these results demonstrated that the truncation of the LDH N-terminal domain does not entirely prevent the protein from forming tetramers. This ability of the truncated dimers to interact and form weak tetramers validated our *in silico* model and provided valuable information about this new tetrameric interface.

Identification of peptide ligands of the LDH tetrameric interface

We then set out to further characterize the continuous epitope **B_1** in order to identify peptides targeting the LDH tetrameric interface. As discussed above, cluster **B_1** corresponds to a 22 amino-acid peptide folding into a long and "kinked" α-helix ended by a short loop (**Figure 3**). We thus decided to study the interaction between "cluster **B_1**"-derived peptide (named **LP-22**, LEDKLKGEMMDLQHGSLFLQTP) and the LDH-H tetrameric interface. To that end, we performed a set of biophysical evaluation using nuclear magnetic resonance (NMR) WaterLOGSY, MST and NanoDSF experiments.

Strikingly, WaterLOGSY experiments showed that **LP-22** undergoes a saturation transfer with dimeric LDH-Htr, but not with the tetrameric LDH-1, thus demonstrating that it interacts at the LDH tetrameric interface (**figure 4a**). MST further validated this interaction with an estimated K_d of 156 µM with LDH-Htr (**figure 4b**). Thermal shift experiments using NanoDSF revealed a stabilization (ΔTm = 2.8°C at 500 µM) (**figure 4d**) of dimeric truncated LDH-Htr with **LP-22**, consistent with an interaction occurring at the exposed oligomeric interface and with the stabilization that usually follows a ligand-protein interaction due to an increase in its Gibbs free energy of unfolding.[45] On the opposite, **LP-22** destabilized tetrameric LDH in a concentration-dependent manner (**Figure 4e** and **4f**) with an EC_{50} = 47 µM [32 to 68 µM]. These results are coherent with the observation that ligands interacting at oligomeric interfaces often induce protein thermal destabilization.[46] The LDH-5 tetramer was more destabilized than LDH-1, consistent with a difference in the stability of these two protein complexes that we previously reported (**Figure S2**).[16] Interestingly, a recent report of selective LDH-5 inhibitors disclosed an inhibitor interacting at LDH-5 tetrameric interface near cluster **B**. This inhibitor was highly selective towards LDH-5, which is coherent with the lower stability of LDH-5

tetrameric complex.[36] Such selectivity profile is also consistent with the higher destabilizing effect that **LP-22** displays on LDH-5 compared to LDH-1. Consistently with our previous report on LDH tetramer disruptors,[16] LDH destabilization was also dependent on protein concentration, as an increasing amount of subunit reverted the effect (**Figure S2**). Overall, these results consistently demonstrated that **LP-22** interacts at the LDH tetrameric interface and destabilizes the tetrameric enzyme.

Biophysical and computational experiments identify LP-22 essential binding region

We next compared **LP-22** WaterLOGSY and ^{1}H-NMR spectra. Because WaterLOGSY is a ligand-based NMR spectroscopy that relies on protein-ligand saturation transfer, **LP-22** residues that do not interact with the protein will be absent of the WaterLOGSY spectrum.[47] A careful comparison between **LP-22** ^{1}H and WaterLOGSY spectra highlighted ^{1}H chemical shifts regions characteristic to lysine, glutamate, aspartate, and leucine aliphatic regions that were not undergoing saturation transfer (**figure 5a** and **5b**). Calculation of the contribution of each residue to the peptide-binding free energy further suggested that N-terminal **LP-22** residues LEDKLK, a region rich in those particular amino acids, did not account for much of **LP-22** binding energy (**figure 5c**). Removal of these six N-terminal residues led to **GP-16** (GEMMDLQHGSLFLQTP), a peptide that had a similar WaterLOGSY spectrum (**figure 5a**), thus suggesting that the two peptides were interacting very similarly. MST indicated that the interaction with dimeric LDH was slightly weakened, with a K_d = 240 µM (**Figure S3**). Consistently, nanoDSF established that **GP-16** could still destabilize tetrameric LDH in a concentration-dependent manner (EC_{50} = 262 µM [142 to 383 µM]) (**figure 5d**).

Probing GP-16 and LDH-H Tetrameric Interface Hot Spots

Computational and biophysical data suggested that the **GP-16** sequence represents an essential binding region of the LDH tetrameric interface**.** To verify this hypothesis, we probed the contribution of each residue of cluster $\mathbf{B_1}$ to the stability of LDH-H oligomeric state. To that end, we performed an alanine scanning of the LDH-1 sequence corresponding to **GP-16**. We thus designed, produced and purified the 16 corresponding LDH-H recombinant alanine variants and evaluated these mutants for their thermal and chemical stability (**Figure 6a,b** and **Table 1**). These variants were also evaluated by MP (**Table 1**, **Figure 6c** and **S4**).

Among the different single-point alanine mutations, three of them significantly impacted the LDH-1 oligomeric state, with variants E62A and F72A behaving mainly as dimers in solution, and variant L71A behaving as a mixture of tetramers and dimers according to MP results (**Figure 6c**). Consistently, nanoDSF experiments showed that LDH-H^{F72A} and LDH-H^{E62A} exhibited denaturation patterns comparable to dimeric LDH-Htr, with a lower initial 350/330 nm ratio and a red-shift instead of the blue-shifts usually observed for tetrameric LDH variants (**Figure 6a**). Interestingly, LDH-H^{L71A} exhibited a lower initial ratio and a red-shift as well, but a T_m 10°C higher than LDH-Htr. This mixed profile is coherent with the mixture of dimers and tetramers that appear to be present in solution with this variant. Comparison of the tryptophan fluorescence spectra of these variants with LDH-1 showed decays in fluorescence intensity characteristic of the dimeric forms of LDHs for variants E62A and F72A but not L71A (**Figure 7a**).[16]

Mutations of L73 and D65, two other hot-spots previously suggested by *in silico* analysis, resulted in tetrameric variants displaying a significant reduction of stability as assessed by both thermal and chemical denaturation (**Figure 5** and **Table 1**). In line with the expected reduction of

tetrameric stability, dilution experiments of the D65A variant resulted in concentration-dependent destabilization of the protein and in the apparition of a second unfolding event (**Figure 7b,c**). Interestingly, variants L66A and L73A showed similar stabilities by nanoDSF, with T_m of 61.1 and 62.0 °C, respectively. However, chemical denaturation experiments demonstrated a striking difference in stability between these two mutants, with EC_{50}s of 0.630 and 0.348 M, respectively (**Figure 7d,e** and **Table 1**). MP experiments validated the presence of an equilibrium between dimers and tetramers for L73A, but not for L66A (**Figure S4**). In accordance with our *in silico* calculation and available crystallographic data,[48] these results confirm that mutation L73A reduces LDH-1 oligomeric stability. In contrast, mutation L66A appears to impact the stability of the protein differently, for instance, by disturbing its hydrophobic core. These results further highlight the importance of exploiting orthogonal methods when assessing the impact of a mutation on protein stability. Other mutations resulted in tetrameric proteins displaying a medium to low variation of their chemical and thermal stability compared to wild-type LDH-1, highlighting the lesser importance of these residues for the oligomeric state of the protein (**Table 1**).

Overall, the different stabilities of the mutants coherently matched with our *in silico* prediction of the ΔG of interaction, and highlighted new molecular determinants of the LDH tetrameric interface (**Figure 5c**). Cluster $\mathbf{B_1}$ hot-spots are constituted by the two negatively charged amino-acids, E62 and D65, and by the three consecutive hydrophobic residues: L71, F72 and L73. Based on the crystallographic structure (PDB ID: 1I0Z), E62 and D65 are involved in a hydrogen bond network with water and neighboring residues R170, K246, A252 and W251. L71, F72 and L73 perform hydrophobic interactions between each other and with residues L166, A169, P183, A252 and L255 (**Figure 8**). Interestingly, cluster $\mathbf{B_1}$ is constituted of both polar and apolar hot spots, which contrasts with the purely lipophilic hot spots that we had previously identified in the LDH tetramerization arm.[16] Therefore, we anticipate that **GP-16**-derived peptides represent promising starting points for future optimization towards LDH tetramers disruptors acting at cluster $\mathbf{B_2}$ tetramerization site.

Conclusion

Over the past years, intense efforts were devoted to the development of LDH inhibitors.[17] Unfortunately, the polarity of LDH active site and high intracellular concentrations of the enzyme have challenged the discovery of LDH inhibitors displaying potent and durable *in vivo* inhibition.[29,34] Recently, new advances in the development of ligands targeting LDH oligomeric interface have offered new avenues towards LDH inhibition.[16,35,36] Targeting protein self-association is an emerging concept in drug design that can bring several advantages over classical orthosteric inhibition. First, targeting the LDH oligomeric interface could unravel new allosteric sites, potentially leading to compounds displaying improved drug-like features compare to LDH active site inhibitors. Secondly, molecules interacting at a protein homomeric interface can lead to its destabilization and degradation,[43] providing compounds with a sub-stoichiometric effect. In this study, we report the identification and characterization of a new LDH tetrameric interface and its essential residues, using a combination of MP, nanoDSF and chemical stability experiments. These results are in accordance with previous computational studies that suggested that this region is involved in LDH tetramerization.[35,40] Furthermore, we report the identification of a family of peptidic ligands that target the tetrameric interface of LDH, destabilize the tetrameric LDH, and stabilize the dimeric LDH-Htr. Altogether, this work provides a structural

characterization of the molecular determinant of the LDH tetrameric interface, as well as valuable pharmacological tools for the future development of compounds targeting the LDH oligomeric state.

Experimental procedure

Chemicals and peptides

All reagents were purchased from different chemical suppliers and used without further purification. Peptides were purchased from Genecust (https://www.genecust.com). Structure conformity and purity grade (> 95%) were assessed by analytical high-performance liquid chromatography (HPLC) analysis and mass spectrometry (MS). Peptide **GP-16** was amidated and acetylated respectively at its C- and N-termini and **LP-22** was only amidated at his C-terminus.

Production and purification of human LDH proteins

The *hLDHB* nucleotidic sequences used to produce full-length, truncated and variant LDH-H proteins inserted in a pET-28a expression vector were ordered from Genecust. NdeI and Bpu1102I restriction sites were used for sequence insertion and allowed for an N-terminal 6-His tag addition. Protein production and purification were performed following a previously described procedure.[16] Recombinant plasmids were then transformed in host bacterium *E. coli* Rosetta (DE3). Transformants were cultured in terrific broth (TB) medium supplemented with 50 µg/mL kanamycin and 34 µg/mL chloramphenicol at 37°C until an optical density of 0.8 was reached. LDH expression was induced by the addition of 1 mM isopropyl-β-*D*-1-thiogalactopyranoside (IPTG) at 20°C for 20 h. Then, cells were collected by centrifugation at 5,000 rpm (rotor 11150, Sigma), 4°C for 25 min. Pellets were suspended in a lysis buffer (Tris.HCl 50 mM pH 8.5, $MgCl_2$ 10 mM, NaCl 300 mM, imidazole 5 mM and glycerol 10%), and then disrupted by sonication, followed by centrifugation at 4°C, 10,000 rpm (rotor 12165-H, Sigma) for 30 min. The insoluble fraction was discarded, and 1 µL of β-mercaptoethanol was added per mL of soluble fraction. Purification of recombinant proteins was performed using 1 mL His-trap FF-crude columns (GE Healthcare) according to the manufacturer's instructions. Finally, protein concentrations were measured using the Bradford method with the Protein Assay Kit (Biorad), and sample homogeneity was assessed by sodium dodecyl sulfate−polyacrylamide gel electrophoresis (SDS−PAGE) with Coomassie brilliant blue as a staining agent.

Nuclear magnetic resonance

Human LDH-H (full length and truncated)-6His proteins for 1D NMR were expressed and purified from *E. coli*, as described above. All experiments were performed on an Ascend Avance III 600 MHz system equipped with a broadband cryoprobe (Bruker) following a previously described procedure.[16]

For WaterLOGSY NMR studies, samples were prepared in 10% D_2O containing 50 mM sodium phosphate buffer, pH 7.6, and 100 mM NaCl. The concentration of LDHs was ranging from 15 to 20 µM of monomer. Ligand binding was detected using a WaterLOGSY ephogsygpno.2 avance-version sequence with a 1 s mixing time, 4096 scans were collected at 277K to yield a 16K points free induction decay (FID). Water signal suppression was achieved using an excitation-sculpting scheme, and a 50 ms spinlock was used to suppress protein background signals.

In silico evaluation

Calculation of the free binding energy and mapping of the interaction at LDH interface was performed using the Molecular Operating Environment (MOE) software (ChemComp) with the LDH-1 crystallographic structure (PDB entry 1I0Z).[48] Following a previously described procedure, tetrameric LDH-1 was generated from the PDB crystallographic structure using the MOE bioassembly

tool.[16] The truncated dimeric version of LDH-1 (LDH-Htr) was generated from the tetrameric complex by removing LDH-H subunits **B** and **D**, as well as the N-terminal domain of subunits **A** and **C**[57,60] Minimization was performed before free energy calculation and interaction mapping.

Nano differential scanning fluorimetry experiments

NanoDSF was performed following previously described procedures.[16]

Variant evaluation. Solutions of proteins (LDH-H, LDH-Htr or variants), stored in a 50 mM sodium phosphate, 100 mM NaCl and 20% glycerol, pH 7.6, were evaluated on a Tycho NT.6 device (NanoTemper Technologies) using concentrations ranging from 25 to 65 µM. According to standard manufacturer's procedures, samples were poured into capillaries and heated up to 95°C in 3 min, while following fluorescence emission at 330 and 350 nm. Melting temperatures were extracted from the derivative of the 350/330 nm fluorescence ratios upon increasing temperature.

Peptide evaluation. Solutions of proteins (LDH-1, LDH-5 or LDH-Htr) with peptides were evaluated on a Tycho NT.6 device (NanoTemper Technologies). Evaluations were performed in a 50 mM sodium phosphate and 100 mM NaCl pH 7.6 buffer. According to standard manufacturer's procedures, samples were poured into capillaries and heated up to 95°C in 3 min, while following fluorescence emission at 330 and 350 nm. Melting temperatures were extracted from the derivative of the 350/330 nm fluorescence ratios upon increasing temperature.

Microscale thermophoresis

MST measurements were performed on a Nanotemper Monolith NT.115 instrument (NanoTemper Technologies) using Red-dye-NHS fluorescent labelling. LDH-Htr purified to homogeneity was labelled with the Monolith Red-dye-NHS 2nd generation labelling dye (Nanotemper Technologies), according to the supplied protocol. Measurements were performed in 50 mM sodium phosphate, pH 7.6, and 100 mM NaCl containing 0.01 % Tween-20 in standard-treated capillaries (NanoTemper Technologies). The final concentration of proteins in the assay was 100 nM. Ligands were titrated in 1:1 dilutions following manufacturer's recommendations. Experiments were performed in triplicates using 40% LED power, high MST power, Laser on time 20 s and Laser off time 3 s. Peptides were evaluated for their thermophoretic pattern, and K_d's were extracted from raw data at a 1.5 s MST on time following the manufacturer's instructions.

Mass photometry

Protein landing was recorded using a Refeyn OneMP (Refeyn Ltd., UK) mass photometry system by adding 1 µL of the protein stock solution (1 µM) directly into a 16 µL drop of filtered PBS solution. Movies were acquired for 60 s (6.000 frames) with the AcquireMP (Refeyn Ltd., v2.1.1) software using standard settings. Data were analyzed using default settings on DiscoverMP (Refeyn LTD, v2.1.1).[44] Contrast-to-mass (C2M) calibration was performed prior to the experiments using a mix of proteins with molecular weights of 66 kDa, 146 kDa, 480 kDa and 1048 kDa.

Spectrophotometric experiments

All spectrophotometric experiments were performed with opaque 96-well plates using a Spectramax m2e spectrophotometer (Molecular Devices) following previously described procedures.[16]

Intrinsic fluorescence assays. Full tryptophan fluorescence spectra were recorded using an excitation wavelength of 286 nm and recording the emission spectra from 320 to 400 nm at room temperature. The raw fluorescence of each experiment

was subtracted to a corresponding control experiment without the protein. Experiments were performed in a 50 mM sodium phosphate and 100 mM NaCl, pH 7.6, buffer. For dissociation in subunits, increasing amounts of guanidinium.HCl ranging from 0.3 M to 2 M were put in contact with the studied proteins (1.3 µM), and fluorescence spectra were recorded afterwards.

Statistics

All quantitative data are expressed as means ± SEM. Error bars were sometimes smaller than symbols. *n* refers to the total number of replicates. Data were analyzed using the GraphPad Prism 7.0 software.

Data availability

All data are contained within the manuscript and the supporting information.

Acknowledgments

The authors thank Dr. Jamal El Bakali, Severine Ravez, Vincent Stroobant and Didier Colau for fruitful discussions. Funding sources had no role in study design, data collection and interpretation, or the decision to submit the work for publication.

Author contributions

P.S. and R.F. are co-senior authors. L.T., P.S., and R.F. designed the research. L.T., M.L., K.K., L.B. and E.Y. performed research experiments. L.T., M.L., N.J., J.M and J.W. analyzed the data. L.T., K.K and M.L. set up the experimental methods, and L.T., P.S., and R.F. wrote the paper. All authors approved manuscript content.

Funding and additional information

This work was supported by ERC independent researcher Starting Grant 243188 (TUMETABO), the Belgian Science Policy Office (Belspo; Interuniversity Attraction Pole Grant P7/03), the French Community of Belgium (ARC 14/19- 058), the Belgian *Fonds National de la Recherche Scientifique* (F.R.S.-FNRS; Grants 3.4575.11, 2.5025.12, and 31288018), the Belgian *Fondation contre le Cancer* (Fundamental Research Grant FAF-F/2018/1282), a VIB grant (to J.M.), the Research Foundation-Flanders–Fonds de la Recherche Scientifique Excellence of Science project (30829584, to J.M), and the Belgian Télévie (Grants 7.4611.11, 7.4548.13, 7.4507.14, 7.4647.20 and 7.8504.18). P.S. is a Research Director of the F.R.S.-FNRS. L.T. was a PhD Fellow of the F.R.S.-FNRS and is currently a Postdoctoral Researcher of the Belgian *Fondation contre le Cancer*.

Conflicts of interest

The authors declare the following competing financial interest(s): L.T., L.B., P.S., and R.F. are inventors of European Patent Application EP19172347.7, Lactate dehydrogenase inhibitor polypeptides for use in treatment of cancer; L.T., M.L., P.S., R.F. are inventors of European patent Application EP21154636.1, Polypeptide inhibitors of lactate dehydrogenase activity for use in cancer therapy. Authors declare no other conflicts of interest.

Supporting Information

Supplementary figures.

References

(1) Pavlova, N. N.; Thompson, C. B. The Emerging Hallmarks of Cancer Metabolism. *Cell Metab.* **2016**, *23* (1), 27–47.

(2) Otto Warburg, B.; Wind, F.; Negelein, N. The Metabolism of Tumours in the Body. *J. Gen. Physiol.* **1927**, *8* (6), 519–530.

(3) San-Millán, I.; Brooks, G. A. Reexamining Cancer Metabolism: Lactate Production for Carcinogenesis Could Be the Purpose and Explanation of the Warburg Effect. *Carcinogenesis* **2017**, *38* (2), 119–133.

(4) de Saedeleer, C. J.; Copetti, T.; Porporato, P. E.; Verrax, J.; Feron, O.; Sonveaux, P. Lactate Activates HIF-1 in Oxidative but Not in Warburg-Phenotype Human Tumor Cells. *PLoS One* **2012**, *7* (10), e46571.

(5) Beckert, S.; Farrahi, F.; Aslam, R. S.; Scheuenstuhl, H.; Königsrainer, A.; Hussain, M. Z.; Hunt, T. K. Lactate Stimulates Endothelial Cell Migration. *Wound Repair Regen.* **2006**, *14*, 321–324.

(6) Végran, F.; Boidot, R.; Michiels, C.; Sonveaux, P.; Feron, O. Lactate Influx through the Endothelial Cell Monocarboxylate Transporter MCT1 Supports an NF-KB/IL-8 Pathway That Drives Tumor Angiogenesis. *Cancer Res.* **2011**, *71* (7), 2550–2560.

(7) Izumi, H.; Takahashi, M.; Uramoto, H.; Nakayama, Y.; Oyama, T.; Wang, K. Y.; Sasaguri, Y.; Nishizawa, S.; Kohno, K. Monocarboxylate Transporters 1 and 4 Are Involved in the Invasion Activity of Human Lung Cancer Cells. *Cancer Sci.* **2011**, *102* (5), 1007–1013.

(8) Colen, C. B.; Shen, Y.; Ghoddoussi, F.; Yu, P.; Francis, T. B.; Koch, B. J.; Monterey, M. D.; Galloway, M. P.; Sloan, A. E.; Mathupala, S. P. Metabolic Targeting of Lactate Efflux by Malignant Glioma Inhibits Invasiveness and Induces Necrosis: An in Vivo Study. *Neoplasia* **2011**, *13* (7), 620–632.

(9) Whitaker-Menezes, D.; Martinez-Outschoorn, U. E.; Lin, Z.; Ertel, A.; Flomenberg, N.; Witkiewicz, A. K.; Birbe, R.; Howell, A.; Pavlides, S.; Gandara, R.; Pestell, R. G.; Sotgia, F.; Philp, N. J.; Lisanti, M. P. Evidence for a Stromal-Epithelial "Lactate Shuttle" in Human Tumors. *Cell Cycle* **2011**, *10* (11), 1772–1783.

(10) Colegio, O. R.; Chu, N. Q.; Szabo, A. L.; Chu, T.; Rhebergen, A. M.; Jairam, V.; Cyrus, N.; Brokowski, C. E.; Eisenbarth, S. C.; Phillips, G. M.; Cline, G. W.; Phillips, A. J.; Medzhitov, R. Functional Polarization of Tumour-Associated Macrophages by Tumour-Derived Lactic Acid. *Nature* **2014**, *513*, 559–563.

(11) Doherty, J. R.; Cleveland, J. L. Targeting Lactate Metabolism for Cancer Therapeutics. *J. Clin. Invest.* **2013**, *123* (9), 3685–3692.

(12) Chiarugi, A.; Dölle, C.; Felici, R.; Ziegler, M. The NAD Metabolome - A Key Determinant of Cancer Cell Biology. *Nat. Rev. Cancer* **2012**, *12*, 741–752.

(13) Sonveaux, P.; Végran, F.; Schroeder, T.; Wergin, M. C.; Verrax, J.; Rabbani, Z. N.; De Saedeleer, C. J.; Kennedy, K. M.; Diepart, C.; Jordan, B. F.; Kelley, M. J.; Gallez, B.; Wahl, M. L.; Feron, O.; Dewhirst, M. W. Targeting Lactate-Fueled Respiration Selectively Kills Hypoxic Tumor Cells in Mice. *J. Clin. Invest.* **2008**, *118* (12), 3930–3942.

(14) Brisson, L.; Bański, P.; Sboarina, M.; Dethier, C.; Danhier, P.; Fontenille, M.-J.; Van Hée, V. F.; Vazeille, T.; Tardy, M.; Falces, J.; Bouzin, C.; Porporato, P. E.; Frédérick, R.; Michiels, C.; Copetti, T.; Sonveaux, P. Lactate Dehydrogenase B Controls Lysosome Activity and Autophagy in Cancer. *Cancer Cell* **2016**, *30* (3), 418–431.

(15) Payen, V. L.; Mina, E.; Van Hée, V. F.; Porporato, P. E.; Sonveaux, P. Monocarboxylate Transporters in Cancer. *Mol. Metab.* **2020**, *33*, 48–66.

(16) Thabault, L.; Brisson, L.; Brustenga, C.; Gache, S. A. M.; Kozlova, A.; Spillier, Q.; Liberelle, M.; Benyahia, Z.; Messens, J.; Copetti, T.; Sonveaux, P.; Frédérick, R. Interrogating the Lactate Dehydrogenase Tetramerization Site Using (Stapled) Peptides. *J. Med. Chem.* **2020**, *63* (9), 4628–4643.

(17) Rani, R.; Kumar, V. Recent Update on Human Lactate Dehydrogenase Enzyme 5 (HLDH5) Inhibitors: A Promising Approach for Cancer Chemotherapy. *J. Med. Chem.* **2016**, *59*, 487–496.

(18) Granchi, C.; Bertini, S.; Macchia, M.; Minutolo, F. Inhibitors of Lactate Dehydrogenase Isoforms and Their Therapeutic Potentials. *Curr. Med. Chem.* **2010**, *17*, 672–697.

(19) Xie, H.; Hanai, J. I.; Ren, J. G.; Kats, L.; Burgess, K.; Bhargava, P.; Signoretti, S.; Billiard, J.; Duffy, K. J.; Grant, A.; Wang, X.; Lorkiewicz, P. K.; Schatzman, S.; Bousamra, M.; Lane, A. N.; Higashi, R. M.; Fan, T. W. M.; Pandolfi, P. P.; Sukhatme, V. P.; Seth, P. Targeting Lactate Dehydrogenase-A Inhibits Tumorigenesis and Tumor Progression in Mouse Models of Lung Cancer and Impacts Tumor-Initiating Cells. *Cell Metab.* **2014**, *19* (5), 795–809.

(20) Le, A.; Cooper, C. R.; Gouw, A. M.; Dinavahi, R.; Maitra, A.; Deck, L. M.; Royer, R. E.; Vander Jagt, D. L.; Semenza, G. L.; Dang, C. V. Inhibition of Lactate Dehydrogenase A Induces Oxidative Stress and Inhibits Tumor Progression. *Proc. Natl. Acad. Sci.* **2010**, *107* (5), 2037–2042.

(21) Smith, B.; Schafer, X. L.; Ambeskovic, A.; Spencer, C. M.; Land, H.; Munger, J. Addiction to Coupling of the Warburg Effect with Glutamine Catabolism in Cancer Cells. *Cell Rep.* **2016**, *17* (3), 821–836.

(22) McCleland, M. L.; Adler, A. S.; Shang, Y.; Hunsaker, T.; Truong, T.; Peterson, D.; Torres, E.; Li, L.; Haley, B.; Stephan, J. P.; Belvin, M.; Hatzivassiliou, G.; Blackwood, E. M.; Corson, L.; Evangelista, M.; Zha, J.; Firestein, R. An Integrated Genomic Screen Identifies LDHB as an Essential Gene for Triple-Negative Breast Cancer. *Cancer Res.* **2012**, *72* (22), 5812–5823.

(23) Ždralević, M.; Vučetić, M.; Daher, B.; Marchiq, I.; Parks, S. K.; Pouysségur, J. Disrupting the 'Warburg Effect' Re-Routes Cancer Cells to OXPHOS Offering a Vulnerability Point via 'Ferroptosis'-Induced Cell Death. *Adv. Biol. Regul.* **2018**, *68*, 55–63.

(24) Dragovich, P. S.; Fauber, B. P.; Boggs, J.; Chen, J.; Corson, L. B.; Ding, C. Z.; Eigenbrot, C.; Ge, H.; Giannetti, A. M.; Hunsaker, T.; Labadie, S.; Li, C.; Liu, Y.; Liu, Y.; Ma, S.; Malek, S.; Peterson, D.; Pitts, K. E.; Purkey, H. E.; Robarge, K.; Salphati, L.; Sideris, S.; Ultsch, M.; Vanderporten, E.; Wang, J.; Wei, B.; Xu, Q.; Yen, I.; Yue, Q.; Zhang, H.; Zhang, X.; Zhou, A. Identification of Substituted 3-Hydroxy-2-Mercaptocyclohex-2-Enones as Potent Inhibitors of Human Lactate Dehydrogenase.

Bioorganic Med. Chem. Lett. **2014**, *24* (16), 3764–3771.

(25) Dragovich, P. S.; Fauber, B. P.; Corson, L. B.; Ding, C. Z.; Eigenbrot, C.; Ge, H.; Giannetti, A. M.; Hunsaker, T.; Labadie, S.; Liu, Y.; Malek, S.; Pan, B.; Peterson, D.; Pitts, K.; Purkey, H. E.; Sideris, S.; Ultsch, M.; Vanderporten, E.; Wei, B.; Xu, Q.; Yen, I.; Yue, Q.; Zhang, H.; Zhang, X. Identification of Substituted 2-Thio-6-Oxo-1,6-Dihydropyrimidines as Inhibitors of Human Lactate Dehydrogenase. *Bioorganic Med. Chem. Lett.* **2013**, *23* (11), 3186–3194.

(26) Rupiani, S.; Buonfiglio, R.; Manerba, M.; Di Ianni, L.; Vettraino, M.; Giacomini, E.; Masetti, M.; Falchi, F.; Di Stefano, G.; Roberti, M.; Recanatini, M. Identification of N-Acylhydrazone Derivatives as Novel Lactate Dehydrogenase A Inhibitors. *Eur. J. Med. Chem.* **2015**, *101*, 63–70.

(27) Kohlmann, A.; Zech, S. G.; Li, F.; Zhou, T.; Squillace, R. M.; Commodore, L.; Greenfield, M. T.; Lu, X.; Miller, D. P.; Huang, W. S.; Qi, J.; Thomas, R. M.; Wang, Y.; Zhang, S.; Dodd, R.; Liu, S.; Xu, R.; Xu, Y.; Miret, J. J.; Rivera, V.; Clackson, T.; Shakespeare, W. C.; Zhu, X.; Dalgarno, D. C. Fragment Growing and Linking Lead to Novel Nanomolar Lactate Dehydrogenase Inhibitors. *J. Med. Chem.* **2013**, *56* (3), 1023–1040.

(28) Rai, G.; Brimacombe, K. R.; Mott, B. T.; Urban, D. J.; Hu, X.; Yang, S. M.; Lee, T. D.; Cheff, D. M.; Kouznetsova, J.; Benavides, G. A.; Pohida, K.; Kuenstner, E. J.; Luci, D. K.; Lukacs, C. M.; Davies, D. R.; Dranow, D. M.; Zhu, H.; Sulikowski, G.; Moore, W. J.; Stott, G. M.; Flint, A. J.; Hall, M. D.; Darley-Usmar, V. M.; Neckers, L. M.; Dang, C. V.; Waterson, A. G.; Simeonov, A.; Jadhav, A.; Maloney, D. J. Discovery and Optimization of Potent, Cell-Active Pyrazole-Based Inhibitors of Lactate Dehydrogenase (LDH). *J. Med. Chem.* **2017**, *60* (22), 9184–9204.

(29) Billiard, J.; Dennison, J. B.; Briand, J.; Annan, R. S.; Chai, D.; Colón, M.; Dodson, C. S.; Gilbert, S. A.; Greshock, J.; Jing, J.; Lu, H.; McSurdy-Freed, J. E.; Orband-Miller, L. A.; Mills, G. B.; Quinn, C. J.; Schneck, J. L.; Scott, G. F.; Shaw, A. N.; Waitt, G. M.; Wooster, R. F.; Duffy, K. J. Quinoline 3-Sulfonamides Inhibit Lactate Dehydrogenase A and Reverse Aerobic Glycolysis in Cancer Cells. *Cancer Metab.* **2013**, *1* (1), 19.

(30) Altamimi, A. M. S.; Alafeefy, A. M.; Balode, A.; Vozny, I.; Pustenko, A.; El Shikh, M. E.; Alasmary, F. A. S.; Abdel-Gawad, S. A.; Žalubovskis, R. Symmetric Molecules with 1,4-Triazole Moieties as Potent Inhibitors of Tumour-Associated Lactate Dehydrogenase-A. *J. Enzyme Inhib. Med. Chem.* **2018**, *33* (1), 147–150.

(31) Boudreau, A.; Purkey, H. E.; Hitz, A.; Robarge, K.; Peterson, D.; Labadie, S.; Kwong, M.; Hong, R.; Gao, M.; Del Nagro, C.; Pusapati, R.; Ma, S.; Salphati, L.; Pang, J.; Zhou, A.; Lai, T.; Li, Y.; Chen, Z.; Wei, B.; Yen, I.; Sideris, S.; McCleland, M.; Firestein, R.; Corson, L.; Vanderbilt, A.; Williams, S.; Daemen, A.; Belvin, M.; Eigenbrot, C.; Jackson, P. K.; Malek, S.; Hatzivassiliou, G.; Sampath, D.; Evangelista, M.; O'Brien, T. Metabolic Plasticity Underpins Innate and Acquired Resistance to LDHA Inhibition. *Nat. Chem. Biol.* **2016**, *12* (10), 779–786.

(32) Oshima, N.; Ishida, R.; Kishimoto, S.; Beebe, K.; Brender, J.; Yamamoto, K.; Urban, D.; Rai, G.; Johnson, M. S.; Benavides, G.; Squadrito, G.; Crooks, D.; Jackson, J.; Joshi, A.; Mott, B. T.; Shrimp, J.; Moses, M. A.; Lee, M.-J.; Yuno, A.; Lee, T.; Hu, X.; Anderson, T.; Kusewitt, D.; Hathaway, H. H.; Jadhav, A.; Picard, D.; Trepel, J.; Mitchell, J. B.; Stott, G.; Moore, W.; Simeonov, A.; Sklar, L.; Norenberg, J.; Maloney,

D. J.; Dang, C. V.; Waterson, A.; Hall, M.; Darley-Usmar, V.; Krishna, M. C.; Neckers, L. Dynamic Imaging of LDH Inhibition in Tumors Reveals Rapid in Vivo Metabolic Rewiring and Vulnerability to Combination Therapy. *Cell Rep.* **2020**, *30* (6), 1798–1810.

(33) Vander Jagt, D.; Deck, L.; Royer, R. Gossypol Prototype of Inhibitors Targeted to Dinucleotide Folds. *Curr. Med. Chem.* **2000**, *7* (4), 479–498.

(34) Ward, R. A.; Brassington, C.; Breeze, A. L.; Caputo, A.; Critchlow, S.; Davies, G.; Goodwin, L.; Hassall, G.; Greenwood, R.; Holdgate, G. A.; Mrosek, M.; Norman, R. A.; Pearson, S.; Tart, J.; Tucker, J. A.; Vogtherr, M.; Whittaker, D.; Wingfield, J.; Winter, J.; Hudson, K. Design and Synthesis of Novel Lactate Dehydrogenase A Inhibitors by Fragment-Based Lead Generation. *J. Med. Chem.* **2012**, *55* (7), 3285–3306.

(35) Jafary, F.; Ganjalikhany, M. R.; Moradi, A.; Hemati, M.; Jafari, S. Novel Peptide Inhibitors for Lactate Dehydrogenase A (LDHA): A Survey to Inhibit LDHA Activity via Disruption of Protein-Protein Interaction. *Sci. Rep.* **2019**, *9* (1), 4686.

(36) Friberg, A.; Rehwinkel, H.; Nguyen, D.; Quanz, M.; Heisler, I.; Langer, G. Structural Evidence for Isoform-Selective Allosteric Inhibition of Lactate Dehydrogenase A. *ACS Omega* **2020**, *5* (22), 13034–13041.

(37) Chung, T. W.; Kim, E. Y.; Han, C. W.; Park, S. Y.; Jeong, M. S.; Yoon, D.; Choi, H. J.; Jin, L.; Park, M. J.; Kwon, Y. J.; Lee, H.; Kim, K. J.; Park, K. H.; Kim, S.; Jang, S. B.; Ha, K. T. Machilin a Inhibits Tumor Growth and Macrophage M2 Polarization through the Reduction of Lactic Acid. *Cancers (Basel).* **2019**, *11* (7), 963.

(38) Qi, J.; Dong, Z.; Liu, J.; Peery, R. C.; Zhang, S.; Liu, J. Y.; Zhang, J. T. Effective Targeting of the Survivin Dimerization Interface with Small-Molecule Inhibitors. *Cancer Res.* **2016**, *76* (2), 453–462.

(39) Gunderwala, A. Y.; Nimbvikar, A. A.; Cope, N. J.; Li, Z.; Wang, Z. Development of Allosteric BRAF Peptide Inhibitors Targeting the Dimer Interface of BRAF. *ACS Chem. Biol.* **2019**, *14* (7), 1471–1480.

(40) Schmidt, R. K.; Gready, J. E. Molecular Dynamics Simulations of L-Lactate Dehydrogenase: Conformation of a Mobile Loop and Influence of the Tetrameric Protein Environment. *J. Mol. Model.* **1999**, *5*, 153–168.

(41) Jaenicke, R.; Vogel, W.; Rudolph, R. Dimeric Intermediates in the Dissociation of Lactic Dehydrogenase. *Eur. J. Biochem.* **1981**, *114* (3), 525–531.

(42) Chemical Computing Group ULC, 1010 Sherbooke St. West, Suite #910, Montreal, QC, Canada, H. 2R7. *Molecular Operating Environment (MOE), 2019.01*; **2020**.

(43) Thabault, L.; Liberelle, M.; Frédérick, R. Targeting Proteins Self-Association in Drug Design. *Drug Discov. Today* **2021**. DOI : 10.1016/j.drudis.2021.01.028.

(44) Young, G.; Hundt, N.; Cole, D.; Fineberg, A.; Andrecka, J.; Tyler, A.; Olerinyova, A.; Ansari, A.; Marklund, E. G.; Collier, M. P.; Chandler, S. A.; Tkachenko, O.; Allen, J.; Crispin, M.; Billington, N.; Takagi, Y.; Sellers, J. R.; Eichmann, C.; Selenko, P.; Frey, L.; Riek, R.; Galpin, M. R.; Struwe, W. B.; Benesch, J. L. P.; Kukura, P. Quantitative Mass Imaging of Single Biological Macromolecules. *Science* **2018**, *360* (6387), 423–427.

(45) Niesen, F. H.; Berglund, H.; Vedadi, M. The Use of Differential Scanning Fluorimetry to Detect Ligand Interactions That Promote Protein Stability. *Nat. Protoc.* **2007**, *2* (9), 2212–2221.

(46) Seetoh, W. G.; Abell, C. Disrupting the Constitutive, Homodimeric Protein-Protein Interface in CK2β Using a Biophysical Fragment-Based Approach. *J. Am. Chem. Soc.* **2016**, *138* (43), 14303–14311.

(47) Dalvit, C.; Pevarello, P.; Tatò, M.; Veronesi, M.; Vulpetti, A.; Sundström, M. Identification of Compounds with Binding Affinity to Proteins via Magnetization Transfer from Bulk Water. *J. Biomol. NMR.* **2000**, *18* (1), 65–68.

(48) Read, J. A.; Winter, V. J.; Eszes, C. M.; Sessions, R. B.; Brady, R. L. Structural Basis for Altered Activity of M□and H□isozyme Forms of Human Lactate Dehydrogenase. *Proteins Struct. Funct. Bioinforma.* **2001**, *43* (2), 175–185.

(49) Appella, E.; Markert, C. L. Dissociation of Lactate Dehydrogenase into Subunits with Guanidine Hydrochloride. *Biochem. Biophys. Res. Commun.* **1961**, *6* (3), 171–176.

Abbreviations

TCA, tricarboxylic acid; LDH, lactate dehydrogenase; LDH-H, lactate dehydrogenase heart isozyme ; LDH-M, lactate dehydrogenase muscle isozyme; LDH-1, lactate dehydrogenase heart isozyme homotetramer; LDH-5, lactate dehydrogenase muscle isozyme homotetramer ; LDHA, lactate dehydrogenase M gene; LDHB, lactate dehydrogenase H gene ; ADME, absorption, distribution, metabolization and excretion; LDH-Htr, LDH-H truncated ; SEC, size-exclusion chromatography ; MST, microscale thermophoresis ; NanoDSF, nanoscale differential scanning fluorimetry ; MP, mass photometry ; NMR, nuclear magnetic resonance ; MOE, Molecular Operating Environment ; ΔTm, thermal shift ; WaterLOGSY, water-ligand observed via gradient spectroscopy; Mw, molecular weight; HPLC, high-performance liquid chromatography; MS, mass spectrometry; TB, terrific broth; IPTG, isopropyl-β-*D*-1-thiogalactopyranoside; SDS-PAGE, sodium dodecyl sulfate−polyacrylamide gel electrophoresis ; FID, free induction decay ; SEM, standard error of the mean; CI95%, confidence interval at 95%; LED, light-emitting diode; K_d, dissociation constant; RFU, relative fluorescent unit; λ_{exc}, wavelength of excitation; λ_{em}, wavelength of emission; kDa, kilodalton.

Table

Table. 1 Oligomeric State and Stability of LDH-H Variants*

	Mw (kDa)	EC_{50} (M)	Tm (°C)	Ratio 350/330 nm
LDH-1	155 ± 17	0.953 ± 0.012	74,5 ± 0,1	1.04
LDH-Htr	88 ± 13	< 0.1	57.5 ± 0.1	0.87
G61A	142 ± 10	0.735 ± 0.018	69.8 ± 0.1	1.05
E62A	77 ± 18	< 0.1	58.9 ± 0.1	0.95
M63A	141 ± 14	0.891 ± 0.012	71.6 ± 0.1	1.04
M64A	149 ± 18	0.845 ± 0.010	68.7 ± 0.1	1.04
D65A	143 ± 12	0.521 ± 0.012	56.4 ± 0.1	1.03
L66A	137 ± 23	0.630 ± 0.011	61.1 ± 0.1	1.03
Q67A	134 ± 16	0.893 ± 0.010	73.1 ± 0.1	1.04
H68A	154 ± 15	0.619 ± 0.016	67.2 ± 0.2	1.05
G69A	153 ± 18	0.722 ± 0.015	73.5 ± 0.1	1.05
S70A	144 ± 13	0.580 ± 0.009	66.0 ± 0.1	1.04
L71A	148 ± 12	< 0.1	67.1 ± 0.1	0.90
F72A	70 ± 17	< 0.1	53.9 ± 0.1	0.94
L73A	137 ± 10	0.348 ± 0.008	62.0 ± 0.1	1.03
Q74A	143 ± 10	0.636 ± 0.020	71.3 ± 0.1	1.05
T75A	145 ± 10	0.439 ± 0.012	64.9 ± 0.1	1.04
P76A	142 ± 17	0.752 ± 0.011	72.2 ± 0.1	1.05

* Reported values are means ± SEM for melting temperatures and EC_{50} (n = 6) and means ± SD for the Mw (the values presented here were obtained with MP from one measurement and were repeated at least 3 times with similar results). The reported molecular weights correspond to the main oligomeric state of the protein.

Figure Legends

Figure 1. Interaction mapping of LDH-H tetrameric interface highlights two main clusters. a) (*Left*) X-ray crystallographic structure of LDH-1 (LDH-H_4) as a dimer of dimers with the two dimers colored differently (subunits A, C and B, D). (*Middle*) Model of dimeric LDH-Htr. (*Right*) Model of dimeric LDH-H interacting with a single LDH-H subunit used to highlight LDH tetrameric interface (PDB ID: 1I0Z). b) Mapping of the interaction between an LDH-H subunit (C) and LDH-1 tetrameric interface (dimer B-D) using the MOE software. The x-axis and y-axis represent the residue numbers of dimer B-D and subunit C, respectively. This mapping identifies two clusters of interaction, clusters **A** and **B**. c) Representation of the different domains of native LDH-1 (UniProt P07195). Residue numbers are scaled to **Figure 1b** x-axis.

Figure 2. LDH-Htr behaves as a weak tetramer. a) Evaluation of LDH-Htr self-interaction using microscale thermophoresis (MST) at a 20 s "on time" ($n = 3$) (K_d = 1.25 µM [0.96 to 1.62 µM]) b) Evaluation by nanoscale differential scanning fluorimetry (NanoDSF) of the impact of LDH-Htr melting temperature depending on its subunit concentration ($n = 3$). T_{m1} and T_{m2} refer to the two transitions observed for LDH-Htr denaturation pattern. c) NanoDSF profile of LDH-Htr at various concentrations ($n = 3$). RFU: Relative fluorescent unit. d) Mass photometry of LDH-Htr with the calculated molecular weights of the complex in solution and their relative intensity indicated above the peaks (theoretical Mw of the dimer is 73.2 kDa).

Figure 3. Structural representation of LDH tetrameric interface shows that cluster B_1 continuous epitope is a long α-helix. Representation of clusters A_1 and B_1 (blue, ribbon) interacting with cluster A_2 and B_2 (orange, surface). The surface corresponds to the molecular surface of LDH-H cluster A_2 and B_2 colored by lipophilicity (Grey-blue: lipophilic; Pink: hydrophilic). This representation was generated from the LDH-1 crystallographic structure and further minimized using Molecular Operating Environment (MOE) software (PDB ID: 1I0Z).

Figure 4. Peptide LP-22 interacts at the LDH tetrameric interface, destabilizes tetrameric LDH and stabilizes dimeric LDH. a) WaterLOGSY spectra of the interaction of **LP-22** (400 µM) with dimeric LDH-Htr (up) and with tetrameric LDH-1 (down) at 15 µM. b) MST binding curves between **LP-22** and LDH-Htr. Binding curves were extracted from the MST traces at a 1.5 s MST on time ($n = 3$). c) NanoDSF denaturation of dimeric LDH-Htr (15 µM) with (red) and without (teal) **LP-22** (500 µM) (ΔTm = 2.8 °C $n = 3$). d) NanoDSF denaturation of tetrameric LDH-5 (300 nM) with (red) and without (teal) **LP-22** (250 µM) (ΔTm = -4.3 °C $n = 3$). e) ΔTm (°C) of tetrameric LDH-5 (300 nM) as a function of **LP-22** concentration (EC_{50} = 47 µM [32 to 68 µM], $n = 3$).

Figure 4. Peptide LP-22 interacts at the LDH tetrameric interface, destabilizes tetrameric LDH and stabilizes dimeric LDH. a) WaterLOGSY spectra of the interaction of **LP-22** (400 µM) with dimeric LDH-Htr (up) and with tetrameric LDH-1 (down) at 15 µM. b) MST binding curves between **LP-22** and LDH-Htr. Binding curves were extracted from the MST traces at a 1.5 s MST on time ($n = 3$). c) NanoDSF denaturation of dimeric LDH-Htr (15 µM) with (red) and without (teal) **LP-22** (500 µM) (ΔTm = 2.8 °C $n = 3$). d) NanoDSF denaturation of tetrameric LDH-5 (300 nM) with (red) and without (teal) **LP-22** (250 µM) (ΔTm = -4.3 °C $n = 3$). e) ΔTm (°C) of tetrameric LDH-5 (300 nM) as a function of **LP-22** concentration (EC_{50} = 47 µM [32 to 68 µM], $n = 3$).

Figure 6. Mutations of cluster B_1 unravel key residues for LDH tetramerization. a) Screening of LDH-H variants using nanoDSF. Changes in the 350/330 nm fluorescence emission indicate blue or red-shifts and are representative of unfolding events ($n = 6$). b) Dissociation of the homotetrameric form of LDH-H and of its variants at 50 µg/mL (1.3 µM) upon addition of guanidinium·HCl. Tryptophan fluorescence intensity was followed at λ_{exc} = 286 nm, λ_{em} = 350 nm as a direct reporter of LDH-1 tetrameric integrity ($n = 6$).[49] c) Mass photometry was performed for different LDH-H variants with the experimental molecular weights of the complexes in solution and their relative intensities. Theoretical molecular weight of the tetramer = 155 kDa; Theoretical molecular weight of the dimer = 78 kDa. Profiles of the other variants can be found in **Figure S4**.

Figure 7. The exploitation of orthogonal methods highlights the impact of key mutations on LDH-H tetrameric stability. a) Tryptophan fluorescence spectra of different LDH-H variants (1.3 μM). λ_{exc} = 286 nm (*n = 6*). b) NanoDSF profiles of LDH-H^{D65A} and LDH-Htr (*n* = 6). c) NanoDSF profile of LDH-H^{D65A} at different concentrations. Data are represented as the derivative of the 350/330 nm fluorescence ratio to highlight the apparition of the second unfolding event (*n = 3*). d) NanoDSF profiles of LDH-H^{L66A} and LDH-H^{L73A} (*n = 6*). e) Fluorescence intensity of tetrameric LDH-H^{L66A} and LDH-H^{L73A} at 50 μg/mL (1.3 μM) upon addition of guanidinium·HCl (*n = 6*).

Figure 8. Structural model of the interaction between cluster B_1 hot spots and cluster B_2. a) Interaction of the sequence corresponding to peptide **GP-16** with cluster $\mathbf{B_2}$. The surface corresponds to the molecular surface of LDH-H cluster $\mathbf{B_2}$ colored for lipophilicity (Grey-blue: lipophilic; Pink: hydrophilic). b) Focus on the hydrophobic hot spot of cluster $\mathbf{B_1}$ with the interaction made by L71, F72 and L73 (blue) with cluster $\mathbf{B_2}$ (orange). c) Focus on the hydrophilic hot spot of cluster $\mathbf{B_1}$ with the interaction made by D65 and E62 (blue) with cluster $\mathbf{B_2}$ (orange). This representation was isolated from the LDH-1 crystallographic structure and further minimized using the MOE software (PDB ID: 1I0Z).

Figure captions

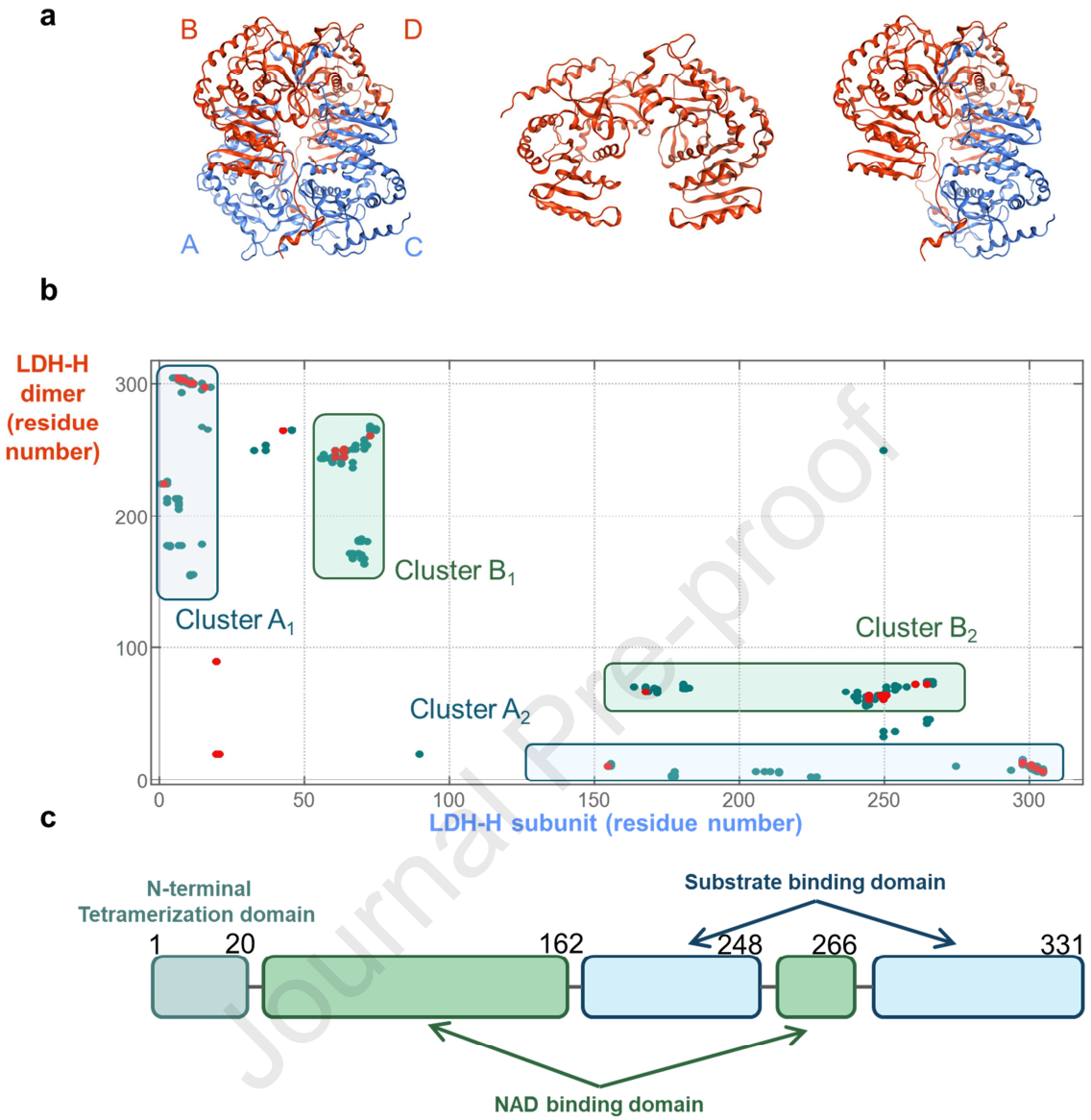

Figure 1.

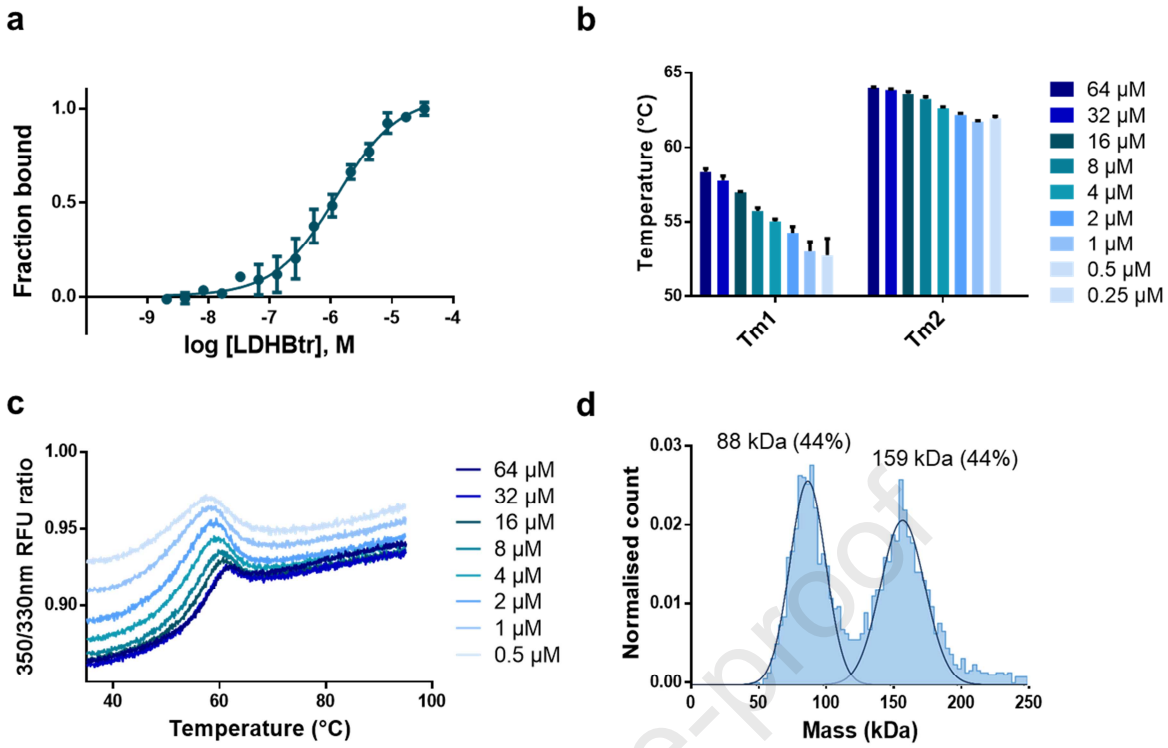

Figure 2.

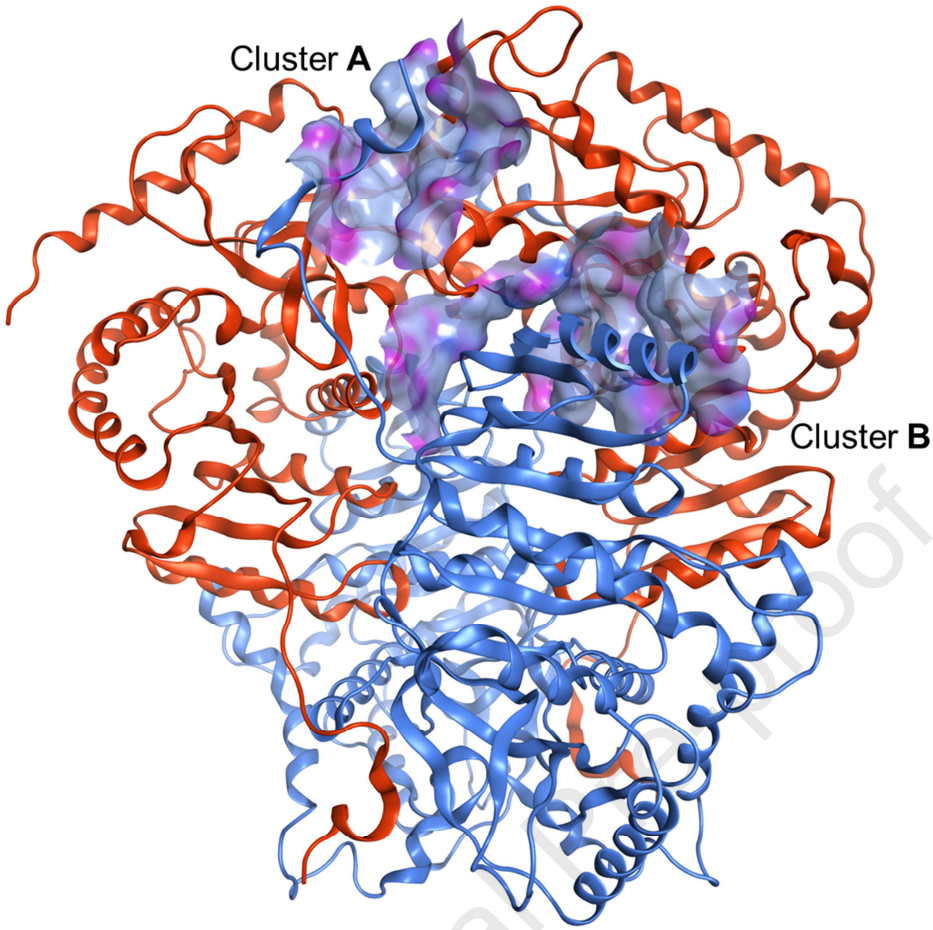

Figure 3.

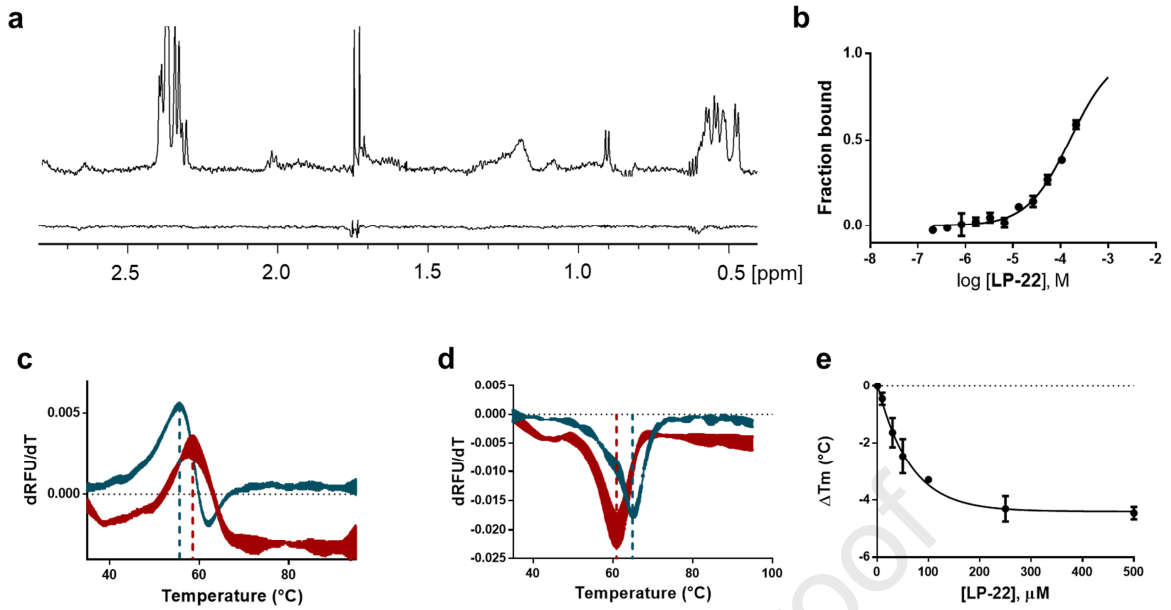

Figure 4.

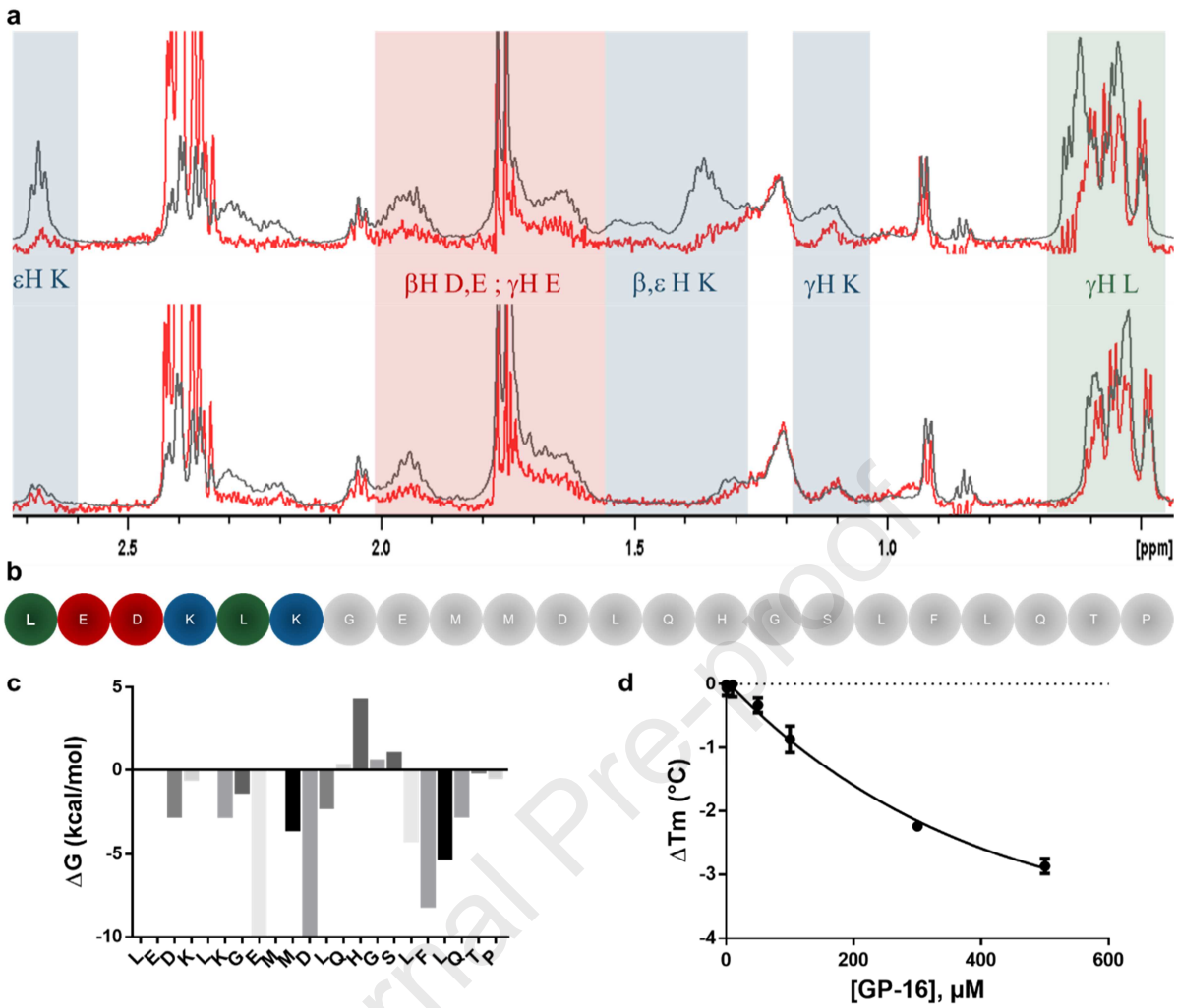

Figure 5.

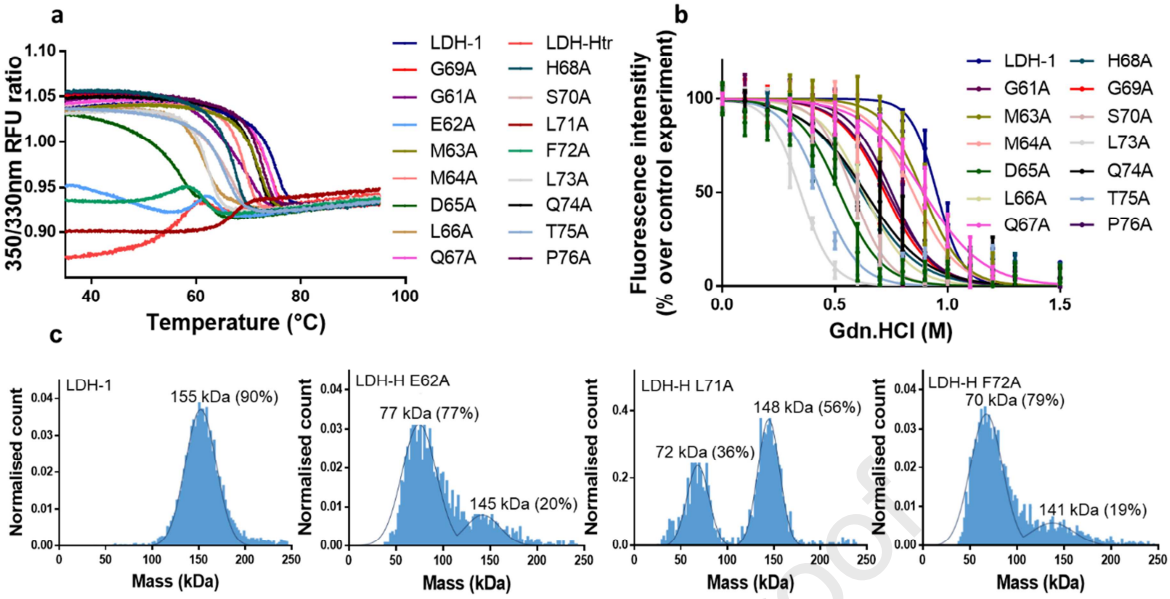

Figure 6.

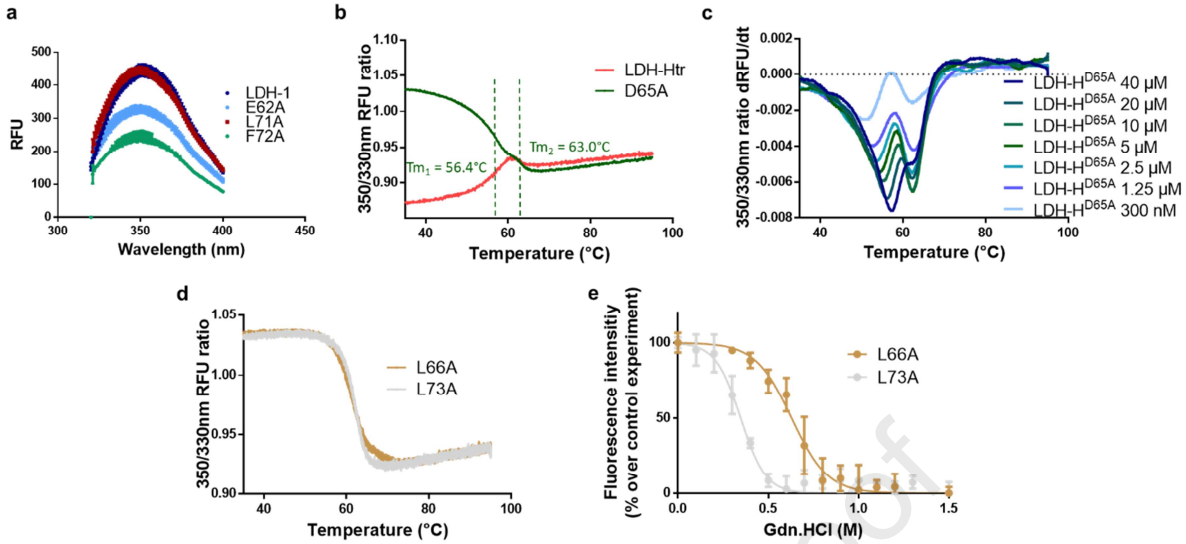

Figure 7.

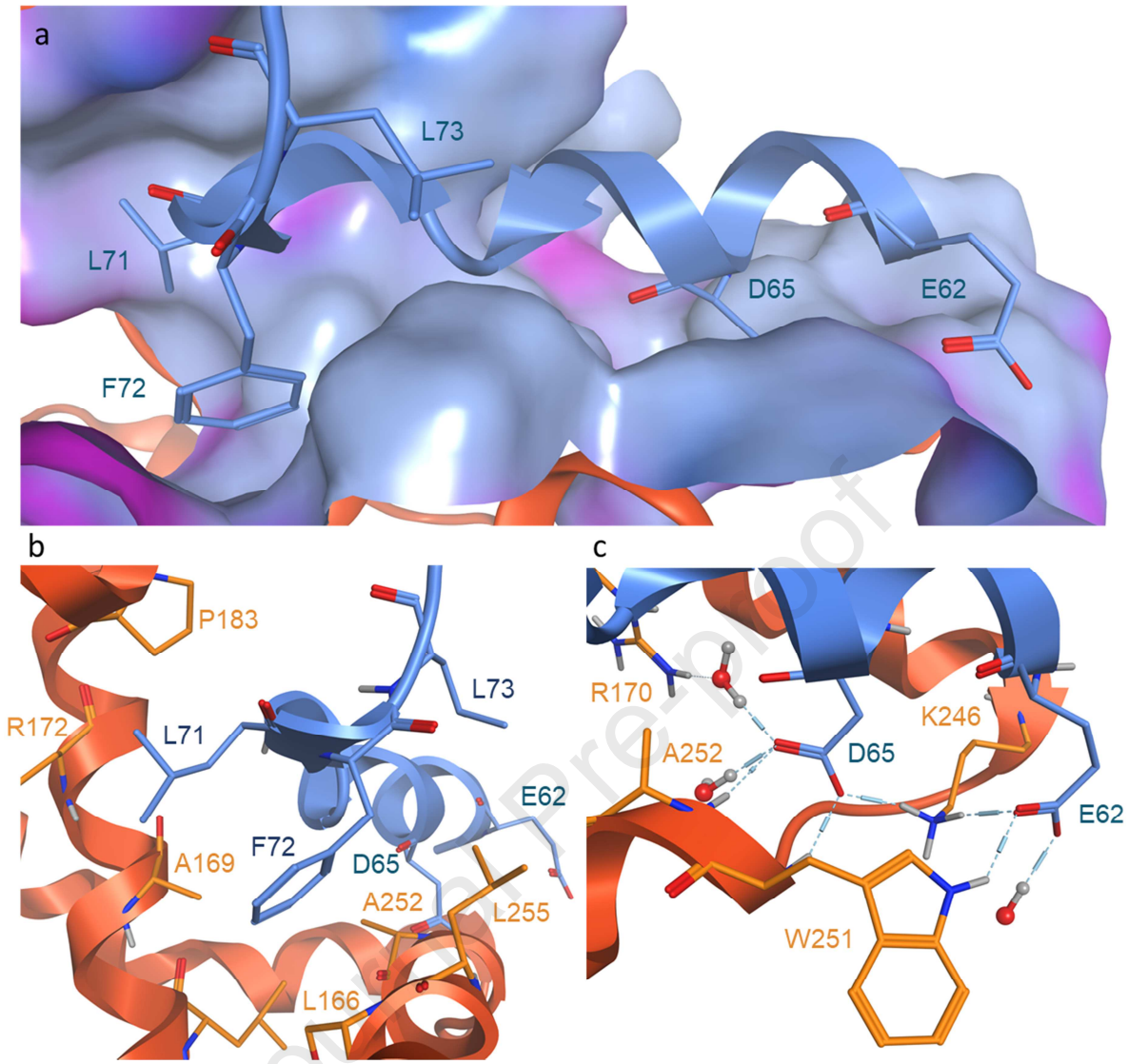

Figure 8.